Results in Physics 6 (2016) 1109–1125

Contents lists available at ScienceDirect

Results in Physics

journal homepage: www.journals.elsevier.com/results-in-physics

Peristalsis of nonconstant viscosity Jeffrey fluid with nanoparticles

N. Alvi [a,*], T. Latif [a], Q. Hussain [a], S. Asghar [a,b]

[a] Department of Mathematics, COMSATS Institute of Information Technology, Islamabad 44000, Pakistan
[b] Nonlinear Analysis and Applied Mathematics (NAAM) Research Group, Faculty of Science, King Abdulaziz University, Jeddah 21589, Saudi Arabia

ARTICLE INFO

Article history:
Received 4 October 2016
Received in revised form 16 November 2016
Accepted 19 November 2016
Available online 27 November 2016

Keywords:
Nanoparticles
Non-Newtonian fluid
Variable viscosity
Viscous dissipation
Mixed convection
Heat transfer
Peristalsis

ABSTRACT

Mixed convective peristaltic activity of variable viscosity nanofluids is addressed. Unlike the conventional consideration of constant viscosity; the viscosity is taken as temperature dependent. Constitutive relations for linear viscoelastic Jeffrey fluid are employed and uniform magnetic field is applied in the transverse direction. For nanofluids, the formulation is completed in presence of Brownian motion, thermophoresis, viscous dissipation and Joule heating. Consideration of temperature dependence of viscosity is not a choice but the realistic requirement of the wall temperature and the heat generated due to the viscous dissipation. Well established large wavelength and small Reynolds number approximations are invoked. Non-linear coupled system is analytically solved for the convergent series solutions identifying the interval of convergence explicitly. A comparative study between analytical and numerical solution is made for certainty. Influence of the parameters undertaken for the description of the problem is pointed out and its physics explained.

Introduction

Heat transfer in peristalsis is undoubtedly an emerging research area due to its vast applications in biomechanics and engineering. Many devices like heart lungs machine, finger and roller pumps operate on the principle of peristalsis. Its further biological relevance lies in the processes of oxygenation and hemodialysis. The literature on the peristaltic flow with heat transfer is quite extensive and a few representative studies are given in [1–6].

The non-Newtonian fluids are now considered to be more realistic in view of the rheological properties shown by industrial, polymeric and physiological fluids. An important class of these non-Newtonian fluids constitute linear viscoelastic model. The base fluid, in this paper, is taken as polymeric fluid with small displacement gradients and the flow constitute small harmonic oscillations. This allows us to take the general viscoelastic fluid as Jeffrey fluid with its appropriate constitutive equations. We know that in this type of model the viscosity remains constant and shear rate is time dependent. However, this viscosity is better taken as a function of temperature which is the crux of this study. We further argue that this model covers a good range of polymeric liquids. To further our argument in favor of the linear viscoelastic model lies in that: it provides the mathematical insight and act as precursor to take up the study in nonlinear viscoelastic models such as second and third grade fluids. Another good reason is that the Jeffrey fluid shows relaxation and retardation time behavior. Some studies regarding Jeffrey fluid by Hayat et al. can be cited in [7–9].

Further, now it is well recognized that the base fluids like water, ethylene glycol have poor heat transfer properties and low thermal conductivity. To overcome limitations of the heat transfer capabilities Maxwell was the first to propose the addition of solid particles and carbon nano-tubes in the base fluid. The results were very encouraging but posed serious issues like erosion of pipes, increase in pressure drop, and clogging. Choi [10] was first to introduce nano scale metallic particles and carbon nano-tubes in the base fluid resulting in what is known as nanofluid. Buongiorno [11] developed the convective heat transfer in nanofluids by making a comprehensive survey. He developed a new model based on the observation that nanoparticle absolute velocity can be viewed as the sum of base fluid velocity and a relative velocity called slip velocity. Finally, he concluded that Brownian diffusion and thermophoresis phenomenon are most important in contributing to heat transfer enhancement. A good number of papers (e.g., [12–14]) have appeared using Buongiornos model for nanofluids.

Magnetic field in nanofluids is significant in medical applications including modern drug delivery and cancer therapy [15]. Cancer patients are administered radiation using iron based nanoparticles and the nanofluids having magnetic properties stick to tumor cells without damaging healthy cells. With this point of view, researches have made some useful contributions in the

* Corresponding author.
E-mail addresses: nida.nisar83@gmail.com, nidanisaralvi@hotmail.com (N. Alvi).

http://dx.doi.org/10.1016/j.rinp.2016.11.045
2211-3797/

theory of nanofluids taking into account Brownian motion and thermopherosis [16–18].

Literature survey reveals that the viscosity of the base fluid in existing literature is mostly taken as constant which is not a valid approximation when the fluid is non- isothermal. This assumption can lead to serious inadequacies because viscosity varies with temperature that greatly affects the fluid flow. The viscous dissipation term is nonzero even for unidirectional flows indicating that there is kinetic energy of the flow being converted to heat energy. This suggests that the temperature does not remain constant and that the assumption of isothermal fluid fails to hold. Hence, the consideration of viscous dissipation and Joule heating should accompany while considering temperature dependent viscosity. Unfortunately, very little has been said on the variable temperature viscosity except the papers given in the references [5,19,20].

In the present context, the study of heat transfer analysis along with viscous dissipation for peristaltic flow of a nanofluids in a channel will be incomplete without the consideration of variable viscosity. As already mentioned sizable investigation can be found for the peristaltic flow of nanofluids with constant viscosity but no information exists for the effects of temperature dependent viscosity on peristaltic flow of nanofluid even for Newtonian fluid. The choice of Jeffrey fluid is important because of a number of reasons. The model is appropriate for small displacement velocity gradients and harmonic oscillations and the viscoelastic properties of the fluid show relaxation and retardation time. The Newtonian fluid can be recovered as a special case and the mathematical ingenuity developed here will lead us to the consideration of more complex non-linear viscoelastic fluids such as second and third grade fluids. Thus, realizing the importance of peristaltic transport of nanofluids and the variable viscosity; we investigate the influence of variable viscosity on peristaltic flow of Jeffrey fluid with nanoparticles in an asymmetric channel.

The governing transport equations are developed including effects of viscous dissipation and Joule heating. Brownian diffusion and thermophoresis phenomenon are also taken into account as per the model of Buongiorno [11]. The relevant problem is reduced into the wave frame. The convergent solution is obtained by homotopic procedure HAM. The analytical results are illustrated graphically and interpreted physically. There are a number of good reasons to take up this study. Firstly, we model the problem of peristaltic transport of MHD non-Newtonian Jeffrey fluid in the presence of Brownian motion and thermopherosis. Secondly, the dynamic viscosity is taken as a function of temperature. Finally, we remark that the theoretical model has been chosen for small displacement gradients with small amplitude harmonic oscillations giving way to the consideration of Jeffrey fluid. Thus, it can be fairly justified that the findings are true if the mathematical subtleties in the formulation have been observed and the correct mathematical procedure is adopted. Thus in the absence of empiricism of any nature so far; the theoretical results for Jeffrey model for the peristaltic transport of nano fluid with variable properties, presented in this paper, can be believed correct; particularly, when the behavior and the interpretation of the results are as per the physics of the problem and the solution satisfies the boundary value problem.

Statement of the physical model

Consider the two-dimensional peristaltic flow of an incompressible Jeffrey nanofluid in an asymmetric channel of uniform thickness $d_1 + d_2$. The electrically conducting fluid is considered in the presence of uniform magnetic field $\overline{\mathbf{B}}$, applied in the transverse direction of the flow. The motion in the fluid is produced in response to the propagation of two sinusoidal wave trains (of constant speed c) along the channel walls (see Fig. 1). It is further assumed that the right hand side wall temperature is T_0 and the nanoparticle concentration is C_0, while the left hand side wall temperature is T_1 ($> T_0$) and concentration is C_1 ($> C_0$).

The wall surfaces can be expressed mathematically as

$$\overline{H}_1(\overline{X},\bar{t}) = d_1 + b_1\cos\left(\frac{2\pi}{\lambda}(\overline{X}-c\bar{t})\right), \quad \text{(right wall)} \tag{1}$$

$$\overline{H}_2(\overline{X},\bar{t}) = -d_2 - b_2\cos\left(\frac{2\pi}{\lambda}(\overline{X}-c\bar{t})+\phi\right), \quad \text{(left wall)} \tag{2}$$

in which λ is the wavelength, b_1 and b_2 are the waves amplitudes and ϕ ($0 \leqslant \phi \leqslant \pi$) is the phase difference between the waves. The $\overline{X}$–axis represent axial direction of flow and $\overline{Y}$–axis is perpendicular to $\overline{X}$–axis. Further, b_i, d_i ($i = 1, 2$) and ϕ satisfy the condition

$$b_1^2 + b_2^2 + 2b_1b_2\cos\phi \leqslant (d_1+d_2)^2. \tag{3}$$

The conservation of mass, momentum, energy and nanoparticle concentration under above mentioned assumptions may be written as

$$\bar{\nabla}\cdot\overline{\mathbf{V}} = 0, \tag{4}$$

$$\rho_f\frac{d\overline{\mathbf{V}}}{d\bar{t}} = \bar{\nabla}\cdot\bar{\boldsymbol{\tau}} + \overline{\mathbf{J}}\times\overline{\mathbf{B}} + \rho_f g\beta_t(\overline{T}-T_0) + \rho_f g\beta_c(\overline{C}-C_0), \tag{5}$$

$$\rho_f\frac{d\bar{e}}{d\bar{t}} = \bar{\boldsymbol{\tau}}\cdot\overline{\mathbf{L}} + k\bar{\nabla}\cdot(\bar{\nabla}\overline{T}) + \frac{1}{\sigma}(\overline{\mathbf{J}}^2) + \tau_1\rho_f c_f\left[D_B(\bar{\nabla}\overline{C}\cdot\bar{\nabla}\overline{T}) + \frac{D_T}{T_0}(\bar{\nabla}\overline{T}\cdot\bar{\nabla}\overline{T})\right], \tag{6}$$

$$\frac{d\overline{C}}{d\bar{t}} = D_B\bar{\nabla}^2\overline{C} + \frac{D_T}{T_0}\bar{\nabla}^2\overline{T}, \tag{7}$$

where $\overline{\mathbf{V}}$ is the velocity vector, $\overline{P}$ is the pressure, ρ_f is the density of the base fluid, β_t is the coefficient of thermal expansion, β_c is the coefficient of expansion with concentration, g is the acceleration

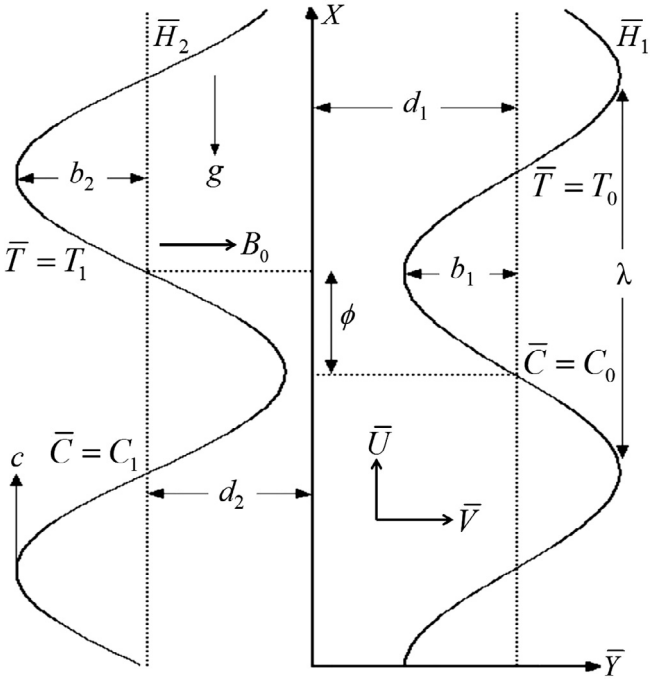

Fig. 1. Geometry of the physical model.

due to gravity, k is the thermal conductivity, $\bar{\mathbf{J}}$ is the Joule current, $\bar{e} = c_f \overline{T}$ is the specific internal energy, c_f is the specific heat capacity of the base fluid, $\overline{T}$ is the temperature, σ is the electrical conductivity of the fluid, $\overline{C}$ is the nanoparticle concentration, $\tau_1 = (\rho c)_p/(\rho c)_f$ is the ratio of the effective heat capacity of the nanoparticle and heat capacity of fluid, D_B is the Brownian diffusion coefficient, D_T is the thermophoretic diffusion coefficient, $\bar{\mathbf{J}} \times \overline{\mathbf{B}}$ is the Lorentz force vector and $\frac{1}{\sigma}\bar{J}^2$ is the Joule heating term. Note that the above equations are subject to the negligibly small magnetic Reynolds number and hence contributions of the induced magnetic field have been ignored. The variations in the magnetic field as a result of both imposed and induced electric fields are also neglected.

The Cauchy stress $\bar{\tau}$ and extra stress $\overline{\mathbf{S}}$ tensors for Jeffrey fluid are given by

$$\bar{\tau} = -\overline{P}\overline{\mathbf{I}} + \overline{\mathbf{S}}, \tag{8}$$

$$\overline{\mathbf{S}} = \frac{\bar{\mu}(\overline{T})}{1+\lambda_1}[\overline{\mathbf{A}}_1 + \lambda_2(\frac{\partial}{\partial \bar{t}} + \overline{\mathbf{V}}\cdot\bar{\nabla})\overline{\mathbf{A}}_1], \tag{9}$$

$$\overline{\mathbf{A}}_1 = \bar{\nabla}\overline{\mathbf{V}} + (\bar{\nabla}\overline{\mathbf{V}})^{\mathrm{T}}, \tag{10}$$

in which $\overline{\mathbf{I}}$ is the identity tensor, λ_1 and λ_2 are the ratio of relaxation to retardation times and the retardation time respectively and $\overline{\mathbf{A}}_1$ is the first Rivlin-Erickson tensor.

The viscosity $\bar{\mu}$ is considered to be variable and is defined by Reynolds law [21] as:

$$\bar{\mu} = \mu_0[1 - \gamma(\overline{T} - T_0)], \tag{11}$$

where μ_0 is the constant viscosity at reference temperature $\overline{T} = T_0$ and γ is a constant.

The velocity ($\overline{\mathbf{V}}$) and magnetic ($\overline{\mathbf{B}}$) fields are defined as

$$\overline{\mathbf{V}} = [\overline{U}(\overline{X},\overline{Y},\bar{t}), \overline{V}(\overline{X},\overline{Y},\bar{t}), 0], \quad \overline{\mathbf{B}} = [0, B_0, 0]. \tag{12}$$

The flow in the fixed reference frame $(\overline{X},\overline{Y},\bar{t})$ appears steady in the wave reference frame $(\bar{x},\bar{y})$. These two frames can be related by the Galilean transformations as

$$(\bar{x},\bar{y}) = (\overline{X} - c\bar{t}, \overline{Y}), \quad (\bar{u},\bar{v}) = (\overline{U} - c, \overline{V}), \quad \bar{p}(\bar{x},\bar{y}) = \overline{P}(\overline{X},\overline{Y},\bar{t}), \tag{13}$$

in which $\bar{u}, \bar{v}$ and $\bar{p}$ are the velocities and pressure with respect to the wave reference frame.

The non-dimensional variables are given below:

$$x = \frac{\bar{x}}{\lambda},\ y = \frac{\bar{y}}{d_1},\ u = \frac{\bar{u}}{c},\ v = \frac{\bar{v}}{c},\ d = \frac{d_2}{d_1},\ a_1 = \frac{b_1}{d_1},\ a_2 = \frac{b_2}{d_1},\ p = \frac{d_1^2\bar{p}}{\mu_0 c\lambda},$$
$$h_1 = \frac{\overline{H}_1}{d_1},\ h_2 = \frac{\overline{H}_2}{d_1},\ \mu(\theta) = \frac{\bar{\mu}(\overline{T})}{\mu_0},\ \theta = \frac{\overline{T}-T_0}{T_1-T_0},\ \eta = \frac{\overline{C}-C_0}{C_1-C_0},\ S = \frac{d_1\bar{S}}{\mu_0 c}. \tag{14}$$

Through Eqs. (4)–(14) we have:

$$\delta\frac{\partial u}{\partial x} + \frac{\partial v}{\partial y} = 0, \tag{15}$$

$$\mathrm{Re}\left(\delta u\frac{\partial u}{\partial x} + v\frac{\partial u}{\partial y}\right) = -\frac{\partial p}{\partial x} + \delta\frac{\partial S_{xx}}{\partial x} + \frac{\partial S_{xy}}{\partial y} - M^2(u+1) + G_t\theta + G_c\eta, \tag{16}$$

$$\mathrm{Re}\delta\left(\delta u\frac{\partial v}{\partial x} + v\frac{\partial v}{\partial y}\right) = -\frac{\partial p}{\partial y} + \delta^2\frac{\partial S_{xy}}{\partial x} + \delta\frac{\partial S_{yy}}{\partial y}, \tag{17}$$

$$\mathrm{RePr}\left(\delta u\frac{\partial\theta}{\partial x} + v\frac{\partial\theta}{\partial y}\right) = \delta^2\frac{\partial^2\theta}{\partial x^2} + \frac{\partial^2\theta}{\partial y^2} + \mathrm{Pr}N_b\left(\delta^2\frac{\partial\eta}{\partial x}\frac{\partial\theta}{\partial x} + \frac{\partial\eta}{\partial y}\frac{\partial\theta}{\partial y}\right)$$
$$+ \mathrm{Br}\left[\delta S_{xx}\frac{\partial u}{\partial x} + S_{yy}\frac{\partial v}{\partial y} + S_{xy}\left(\delta\frac{\partial v}{\partial x} + \frac{\partial u}{\partial y}\right)\right]$$
$$+ \mathrm{Pr}N_t\left[\delta^2\left(\frac{\partial\theta}{\partial x}\right)^2 + \left(\frac{\partial\theta}{\partial y}\right)^2\right] + M^2\mathrm{Br}(u+1)^2, \tag{18}$$

$$\frac{cd_1}{D_B}\left(\delta u\frac{\partial\eta}{\partial x} + v\frac{\partial\eta}{\partial y}\right) = \delta^2\frac{\partial^2\eta}{\partial x^2} + \frac{\partial^2\eta}{\partial y^2} + \frac{N_t}{N_b}\left(\delta^2\frac{\partial^2\theta}{\partial x^2} + \frac{\partial^2\theta}{\partial y^2}\right). \tag{19}$$

In Eqs. (15)–(19), $\delta(= d_1/\lambda)$ is the wave number, $M^2(= \sigma B_0^2 d_1^2/\mu_0)$ is the Hartman number, $\mathrm{Re}(= \rho_f c d_1/\mu_0)$ is the Reynolds number, $\mathrm{Pr}(= \mu_0 c_f/k)$ is the Prandtl number, $\mathrm{Br}(= \mu_0 c^2/(T_1 - T_0)k)$ is the Brinkman Number, $N_t(= \tau_1\rho_f D_T(T_1 - T_0)/\mu_0 T_0)$ is the thermophoresis parameter, $N_b(= \tau_1\rho_f D_B(C_1 - C_0)/\mu_0)$ is the Brownian motion parameter, $G_c(= \rho_f g\beta_c d_1^2(C_1 - C_0)/\mu_0 c)$ is the local concentration Grashof number and $G_t(= \rho_f g\beta_t d_1^2(T_1 - T_0)/\mu_0 c)$ is the local temperature Grashof number.

Now, if we define the stream function ψ as $u = \partial\psi/\partial y$ and $v = -\delta(\partial\psi/\partial x)$, the continuity Eq. (15) is identically satisfied. The long wavelength and low Reynolds number assumption remains applicable for the case of chyme transport in small intestines [22]. In this case $d = 1.25$ cm, $c = 2$ cm/min and $\lambda = 8.01$ cm. Here the half width of the intestine is small as compared to the wavelength. i.e., $d/\lambda = 0.156$. Thus the Eqs. (16)–(19) under the aforementioned assumptions reduce to

$$0 = -\frac{\partial p}{\partial x} + \frac{\partial S_{xy}}{\partial y} - M^2\left(\frac{\partial\psi}{\partial y} + 1\right) + G_t\theta + G_c\eta, \tag{20}$$

$$0 = \frac{\partial^2}{\partial y^2}\left(\mu(\theta)\frac{\partial^2\psi}{\partial y^2}\right) - (1+\lambda_1)M^2\frac{\partial^2\psi}{\partial y^2} + (1+\lambda_1)G_t\frac{\partial\theta}{\partial y} + (1+\lambda_1)G_c\frac{\partial\eta}{\partial y}, \tag{21}$$

$$0 = \frac{\partial^2\theta}{\partial y^2} + \mathrm{Br}S_{xy}\frac{\partial^2\psi}{\partial y^2} + M^2\mathrm{Br}\left(\frac{\partial\psi}{\partial y} + 1\right)^2 + \mathrm{Pr}N_b\left(\frac{\partial\eta}{\partial y}\right)\left(\frac{\partial\theta}{\partial y}\right)$$
$$+ \mathrm{Pr}N_t\left(\frac{\partial\theta}{\partial y}\right)^2, \tag{22}$$

$$0 = \frac{\partial^2\eta}{\partial y^2} + \frac{N_t}{N_b}\left(\frac{\partial^2\theta}{\partial y^2}\right), \tag{23}$$

with

$$S_{xy} = \frac{\mu(\theta)}{(1+\lambda_1)}\frac{\partial^2\psi}{\partial y^2}; \quad \mu(\theta) = 1 - \alpha\theta; \quad \frac{\partial p}{\partial y} = 0,$$

where $\alpha = \gamma(T_1 - T_0)$ is the viscosity parameter.

The boundary conditions are given by

$$\psi = F/2, \quad \frac{\partial\psi}{\partial y} = -1, \quad \theta = 0, \quad \eta = 0, \quad at \quad y = h_1(x)$$
$$= 1 + a_1\cos(2\pi x), \tag{24}$$

$$\psi = -F/2, \quad \frac{\partial\psi}{\partial y} = -1, \quad \theta = 1, \quad \eta = 1 \quad at \quad y = h_2(x)$$
$$= -d - a_2\cos(2\pi x + \phi), \tag{25}$$

in which

$$F=\int_{h_2(x)}^{h_1(x)}\frac{\partial\psi}{\partial y}dy=\psi(h_1(x))-\psi(h_2(x)), \tag{26}$$

is the time averaged flow rate in wave frame. It can be further related by the flow rate in fixed frame by the following expression:

$$Q=F+1+d. \tag{27}$$

The expression for pressure rise per wavelength is

$$\Delta P_\lambda=\int_0^1\left(\frac{dp}{dx}\right)dx. \tag{28}$$

The heat transfer coefficient Z at $y=h_1(x)$ is given by

$$Z=\frac{\partial h_1}{\partial x}\frac{\partial\theta}{\partial y}. \tag{29}$$

Analytical solution

We observed that the Eqs. (20)–(23) are coupled and nonlinear in nature therefore the exact solutions are not possible. Thus, Homotopy Analysis Method is used to obtain the solution as it has the tendency to solve the nonlinear problems. It has significant advantage over other series solution methods in providing simple and efficient way to ensure the convergence of the series solution. We choose the initial guesses for the Homotopic solutions as:

$$\psi_0(y)=-\frac{F(h_1+h_2-2y)(h_1^2-4h_1h_2+h_2^2+2(h_1+h_2)y-2y^2)}{2(h_1-h_2)^3}+\frac{2(h_1+h_2-2y)(h_1-h_2)(h_1-y)(h_2-y)}{2(h_1-h_2)^3}, \tag{30}$$

$$\theta_0(y)=\frac{h_1-y}{h_1-h_2}, \tag{31}$$

$$\eta_0(y)=\frac{h_1-y}{h_1-h_2} \tag{32}$$

The auxiliary linear operators are given below

$$\mathcal{L}_\psi(\psi)=\frac{\partial^4\psi}{\partial y^4},\quad \mathcal{L}_\theta(\theta)=\frac{\partial^2\theta}{\partial y^2},\quad \mathcal{L}_\eta(\eta)=\frac{\partial^2\eta}{\partial y^2}, \tag{33}$$

with the following the properties:

$$\mathcal{L}_\psi(C_1+C_2y+C_3y^2+C_4y^3)=0,\quad \mathcal{L}_\theta(C_5+C_6y)=0,\quad \mathcal{L}_\eta(C_7+C_8y)=0, \tag{34}$$

where C_1-C_8 are arbitrary constants. Further details of the solution procedure are given in Appendix A.

Convergence of HAM solution

As Liao pointed out [23], the convergence of homotopic series solution is strongly dependent on non-zero auxiliary parameters $\hbar_\psi,\hbar_\theta$ and $\hbar_\eta$. The obtain the admissible values of such parameters, the $\hbar$-curves are drawn at 25th order of approximation (see Fig. 2) by choosing some suitable values of other involved parameters. Fig. 2 manifests that the acceptable ranges for $\hbar_\psi,\hbar_\theta$ and $\hbar_\eta$ are $-1.1<\hbar_\psi<-0.3,-1<\hbar_\theta<-0.4$ and $-1<\hbar_\eta<-0.4$. Further, the solutions converge for all values of y when $\hbar_\psi=\hbar_\theta=\hbar_\eta=-0.8$ (Table 1).

Graphical results and discussion

The results obtained in the preceding section are discussed in this section where we recall to have obtained the series solution using Homotopy Analysis Method (HAM). It is worthwhile to supplement the series solution by some numerical study or experimental results. Hence, the numerical solution is also obtained by built in Dopri45 solver that shows an excellent match with the HAM solution (see Table 2). In what follows, we analyzed the different features of the peristaltic transport, heat transfer characteristics and nanoparticle concentration under the effect of various involved parameters namely viscosity parameter α, Brinkman number Br, Brownian motion parameter N_b, thermophoresis parameter N_t, local temperature Grashof number G_t, local nanoparticle Grashof number G_c, Jeffrey fluid parameter λ_1 and Hartman number M.

The aim of Fig. 3 is to see the effects of involving parameters on dp/dx. For this purpose dp/dx is plotted within one wavelength $x\in[-0.5,0.5]$. When pressure gradient is positive, it is called adverse pressure gradient and it resists the flow. In the intervals $x\in[-0.5,-0.3]$ and $x\in[0.2,0.5]$, we have adverse pressure gradient. Here the pressure gradient dp/dx is decreasing by increasing α and λ_1, whereas it is increasing for the rest of the parameters. The negative pressure gradient is called favorable pressure gradient and it assists the flow. Pressure gradient dp/dx is negative for $x\in[-0.3,0.2]$ for all the parameters. Further it is increasing for increasing values of α, Br, N_b,N_t,G_t,G_c and λ_1 while it is decreasing for increasing values of M.

Fig. 4 is sketched in order to study the influence of α, Br, $N_b,N_t,G_t,G_c,\lambda_1$ and M on pressure rise per wavelength ΔP_λ against time-averaged flux Q. We can divide the graph into multiple regions according to the signs of ΔP_λ and Q. The upper left hand region, where $\Delta P_\lambda>0$and $Q<0$ is called retrograde pumping region. The region where $\Delta P_\lambda>0$and $Q>0$ is known as peristaltic pumping region. The lower right hand region where $\Delta P_\lambda<0$and $Q>0$ termed as copumping region. The critical value of Q for which $\Delta P_\lambda=0$ is referred to free pumping flux and is denoted by Q_0. The maximum pressure rise against which peristalsis works as pump, i.e. ΔP_λ for $Q=0$ is denoted by P_0. Fig. 4a and b elucidates that for the increasing values of α and Br pumping decreases in the retrograde and peristaltic pumping regions, however it increases in the copumping region. Also, free pumping flux Q_0 increases (Table 3). Table 4 shows that P_0 decreases by increasing α, hence peristalsis works against less pressure to propel the fluid with variable viscosity as compared to constant viscosity. Decrement in the value of P_0 is observed for rising values of Br (Table 4). Fig. 4c and d shows that retrograde and peristaltic pumping decreases and copumping increases by increasing both N_b and N_t. It is evident from Tables 3 and 4 respectively, that by increasing N_b and N_t, Q_0 increases and P_0 decreases. We can see from Fig. 4e that pumping rate increases in all the regions by increasing G_t. Values of Q_0 and P_0 also increases (Tables 3 and 4) by increasing G_t. The behavior of concentration buoyancy parameter G_c on pressure rise is similar to that accounted for the thermal buoyancy parameter G_t (Fig. 4f). Fig. 4g shows that pumping rate is a decreasing function of λ_1 in the retrograde and peristaltic pumping regions and an increasing function of λ_1 in the copumping region. Free pumping flux Q_0 increases (Table 3) however, maximum pressure rise against which peristalsis works as pump P_0 decreases by increasing λ_1 (Table 4) and thus peristalsis has to work against less pressure in case of non-Newtonian fluid as compared to Newtonian fluid. The variation of ΔP_λ for different values of M is presented in Fig. 4h. It shows that pumping increases in the retrograde pumping region however it decreases in the peristaltic and copumping region. Further Q_0 decreases but P_0 increases by increasing M (Tables 3 and 4).

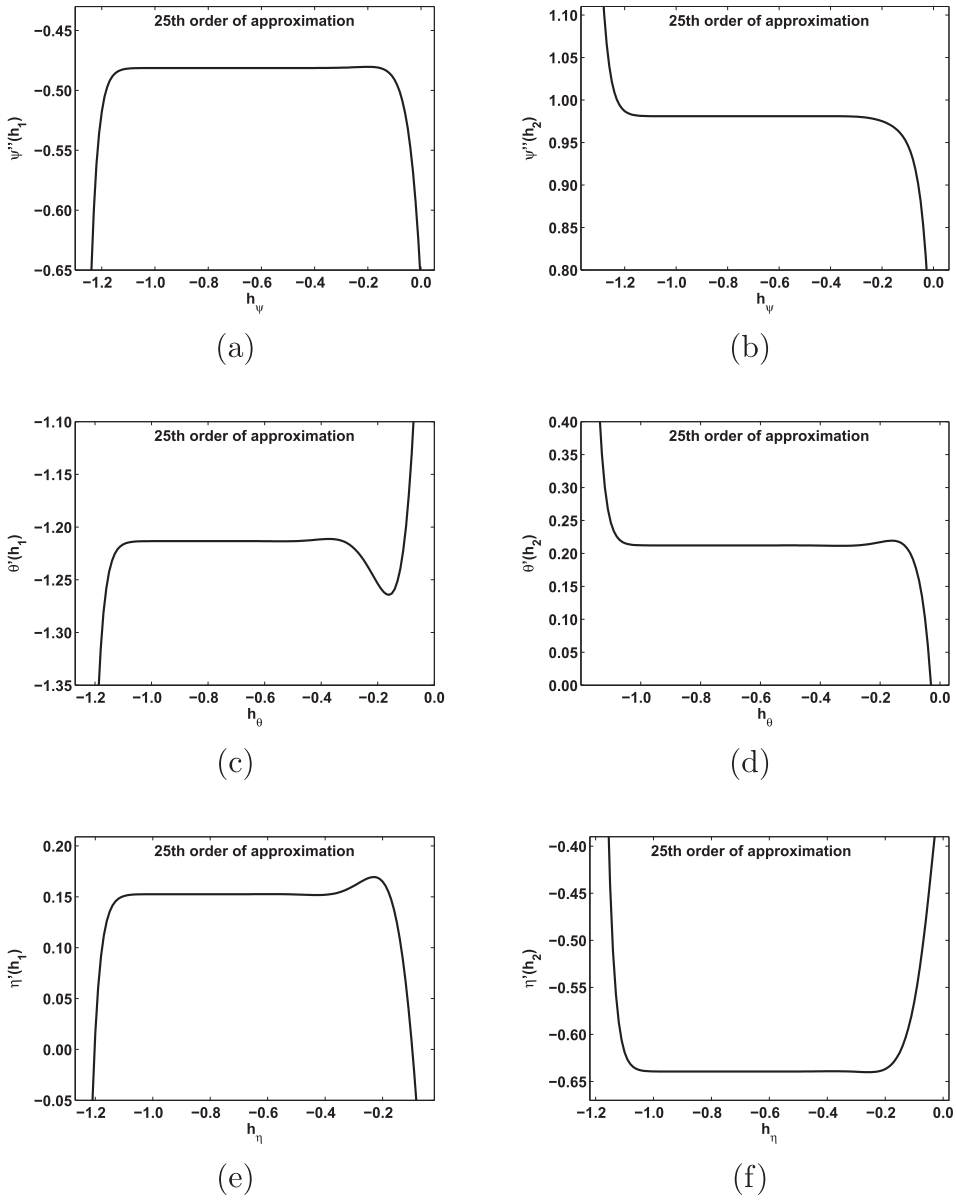

Fig. 2. $\hbar$−curves for ψ, θ and η for $a_1 = 0.5$, $d = 1.5$, $a_2 = 0.5$, $x = 0.1$, $\phi = \pi/4$, $Q = 0.5$, Pr = 1.5, $\alpha = 0.2$, Br = 1, $N_t = 0.5$, $N_b = 0.9$, $G_t = 0.4$, $G_c = 0.4$, $\lambda_1 = 0.2$, $M = 1$.

Table 1
Convergence of HAM solution with $a_1 = 0.5$, $d = 1.5$, $a_2 = 0.5$, $x = 0.1$, $\phi = \pi/4$, $Q = 0.5$, Pr = 1.5, $\alpha = 0.2$, Br = 1, $N_t = 0.5$, $N_b = 0.9$, $G_t = 0.4$, $G_c = 0.4$, $\lambda_1 = 0.2$, $M = 1$, $\hbar_\psi = \hbar_\theta = \hbar_\eta = -0.8$.

No. of iterations	$\psi''(h_1)$	$\theta'(h_1)$	$\eta'(h_1)$	$\psi''(h_2)$	$\theta'(h_2)$	$\eta'(h_2)$
01	−0.53086	−0.91205	−0.33526	0.98334	0.22405	−0.33526
05	−0.47935	−1.30514	0.21004	1.02404	0.22620	−0.64843
10	−0.48137	−1.20440	0.14749	1.03122	0.21117	v0.63808
15	−0.48132	−1.21414	0.15297	1.03096	0.21226	−0.63951
20	−0.48132	−1.21327	0.15252	1.03097	0.21217	−0.63938
25	−0.48132	−1.21334	0.15256	1.03097	0.21217	−0.63940
30	−0.48132	−1.21334	0.15256	1.03097	0.21217	−0.63940

To observe the behavior of velocity profile u with the variation of different parameters, Fig. 5 is sketched. Fig. 5a clearly shows that by increasing the viscosity parameter α, the amplitude of velocity increases as we move closer to the hotter wall (left wall) and it decreases as we move away from it. The reason being the high temperature near the hotter wall, which results in the decrease in viscosity and consequently velocity increases and vice versa. We can see from Fig. 5b that u increases by increasing Br. Since Brinkman number Br is due to the viscous dissipation which means that energy is produced and so the temperature increases and velocity and temperature have direct relation hence velocity increases. N_b is the ratio of diffusion of nanonoparticles due to

Table 2
Comparison of velocity u, temperature θ and concentration η obtained by HAM and numerical dopri45 solver. We choose $a_1 = 0.5$ $d = 1$, $a_2 = 0.5$, $\phi = \pi/2$, $x = 0$, $Q = 1$, M = 1, Pr = 1, Br = 1, $N_b = 0.9$, $N_t = 0.3$, $G_t = 0.1$, $G_c = 0.1$, $\alpha = 0.1$, $\lambda 1 = 0.2$, $\hbar_\psi = \hbar_\theta = \hbar_\eta = -0.8$.

y	HAM	Numerical
(a) Velocity (u)		
−1.00	−1.00000000	−1.00000000
−0.75	−0.64336730	−0.64336732
−0.50	−0.39281976	−0.39281978
−0.25	−0.23003968	−0.23003970
0.00	−0.14190566	−0.14190568
0.25	−0.12022073	−0.12022074
0.50	−0.16115140	−0.16115140
0.75	−0.26472321	−0.26472320
1.00	−0.43440653	−0.43440650
1.25	−0.67664742	−0.67664735
1.50	−1.00000000	−1.00000000
(b) Temperature (θ)		
−1.00	1.00000000	1.00000000
−0.75	1.15903366	1.15903362
−0.50	1.25595774	1.25595771
−0.25	1.30705182	1.30705181
0.00	1.31305637	1.31305638
0.25	1.26868482	1.26868484
0.50	1.16727864	1.16727867
0.75	1.00213070	1.00213075
1.00	0.76494694	0.76494702
1.25	0.44102995	0.44103006
1.50	0.00000000	0.00000000
(c) Concentration (η)		
−1.00	1.00000000	1.00000000
−0.75	0.81365545	0.81365546
−0.50	0.64801408	0.64801409
−0.25	0.49764939	0.49764940
0.00	0.36231454	0.36231454
0.25	0.24377173	0.24377172
0.50	0.14424045	0.14424044
0.75	0.06595643	0.06595642
1.00	0.01168435	0.01168433
1.25	−0.01367665	−0.01367669
1.50	0.00000000	0.00000000

the Brownian motion effect to the momentum diffusion in nanofluid. Similarly, N_t is the ratio of diffusion of nanoparticles due to the thermophoresis force to the momentum diffusion in nanofluid. Effect of N_b and N_t on velocity can be seen in Fig. 5c and d. An increase in velocity is seen by increasing N_b (see Fig. 5c), as the diffusion of particles is increased by increasing Brownian motion parameter N_b. From Fig. 5d we observe that by increasing N_t, the thermophoresis force on the nanoparticles increases which increases the movement of nanoparticles and consequently that leads to fast flow. It is depicted in Fig. 5e that the increase of local temperature Grashof number G_t results in the increase of the velocity of the fluid near the hotter wall. The combined effect of the high temperature of the wall and the increase of temperature gradients results in the enhancement of velocity. Similar behavior of velocity is observed for local nanoparticle Grashof number G_c (see Fig. 5f). Fig. 5g shows the effect of Jeffrey fluid parameter λ_1 on velocity profile. The amplitude of velocity increases near the left wall and decreases near the right wall. Fig. 5h manifests that amplitude of velocity gradually decreases when Hartman number M is increased.

The temperature profile θ is discussed against y for different parameters in Fig. 6. Fig. 6a reveals that the increase of variable viscosity parameter α decreases the temperature profile. Fig. 6b shows that the amplitude of temperature profile increases as a result of increasing Br. The reason being the presence of viscous dissipation term. Due to it, some of the fluid kinetic energy converts to the thermal energy and hence increases the temperature. In nanofluid systems, the Brownian motion and thermophoresis takes place, due to the size of nanoparticles, which has an effect on the heat transfer properties. Fig. 6c and d are prepared to present the effects of N_b and N_t on temperature distribution. It is noted that the increase in N_b leads to an increase in the diffusion of particles, which increases the fluid temperature. Also, by increasing N_t, there is an increase in the thermophoretic force which increases the diffusion of nanoparticles into the fluid and this results in the increase in temperature. Fig. 6e and f elucidates the effect of G_t and G_c on the temperature θ. By increasing G_t and G_c, the temperature decreases near the right wall and the larger values of G_t (or G_c) accompany with the stronger buoyancy force due to temperature gradient (or concentration gradient) rises the temperature near the left wall (hotter wall). Fig. 6g manifests that temperature in the Jeffrey fluid is lower than the temperature in Newtonian fluid. Increase in temperature can be seen by increasing M from Fig. 6h, the reason being the Joule heating effects.

Variation of absolute value of heat transfer coefficient Z for different parameters can be seen in Fig. 7. This figure shows that heat transfer coefficient is positive for $x > 0$ and negative for $x < 0$. This oscillatory behavior is justified in view of peristalsis. Fig. 7a represents that $|Z|$ decreases by increasing viscosity parameter α. This tells that heat transfer coefficient is higher for constant viscosity as compared to variable viscosity. The effect of Br is to increase $|Z|$ as shown in (Fig. 7b). Fig. 7c and d depicts that $|Z|$ shows a similar pattern of increase for both N_b and N_t. Increase in the value of G_t, G_c and λ_1 results in a decrease in $|Z|$ (see Fig. 7g). However opposite behavior is observed for M (Fig. 7h).

Fig. 8 depicts the behavior of different parameters on the nanoparticle volume fraction C. It is clear from Fig. 8a that nanoparticle concentration is increasing by increasing α. Thus variable viscosity fluid concentration is higher as compared to constant viscosity fluid. The presence of viscous dissipation results in the decrease in concentration (see Fig. 8b). It is observed from Fig. 8c and d that the effect of N_b and N_t on the nanoparticle concentration profile η is opposite to that of temperature profile θ. When N_b and N_t are increased, the particle dispersion is higher which results in the decrease in concentration. It can be clearly seen from Fig. 8e that when G_t is increased, the increased temperature gradient results in the dispersion of the concentration distribution species and this results in the decrease in the concentration. Same is true for G_c (Fig. 8f). Concentration in the Jeffrey fluid is higher than the concentration in Newtonian fluid as given in Fig. 8g. Fig. 8h depicts that Hartman number has the same effect on concentration as that of Brinkman number.

The trapping phenomenon is a characteristic feature of peristaltic transport in which streamlines split under certain conditions to trap a bolus. This bolus moves with the same speed as that of wave. The effects of α, Br, $N_b, N_t, G_t, G_c, \lambda_1$ and M on trapping are shown in Figs. 9–16. It is clear that the trapped bolus in the right side increases in size when viscosity parameter α is increased. However, the size of the bolus in the left side decreases. (see Fig. 9). Increasing values of Br have an increasing effect on the size of trapped bolus (Fig. 10). Figs. 11 and 12 indicates that N_b and N_t have negligible effect on trapping phenomenon i.e., the trapping is independent of the consideration of nanoparticles. Figs. 13 and 14 illustrate that increase in both Grashof numbers (G_t and G_c) from zero i.e vanishing buoyancy effects, the volume of trapped bolus clearly increases in right side of the channel and decreases in the left side. As fluid character changes from Newtonian ($\lambda_1 = 0$) to Jeffrey ($\lambda_1 = 1$) (see Fig. 15), the size of trapped bolus decreases. This observation remains true for Fig. 16 which depicts the effects of Hartman number M.

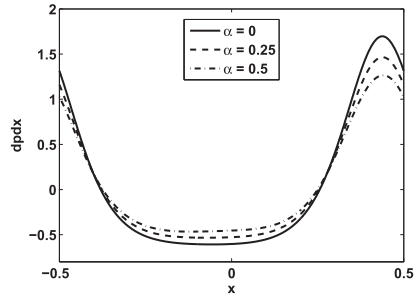

(a) N_b=0.8, N_t=0.7, M=1, Pr=3, Br=1.5, G_t=0.2, G_c=0.2, λ_1=0.1

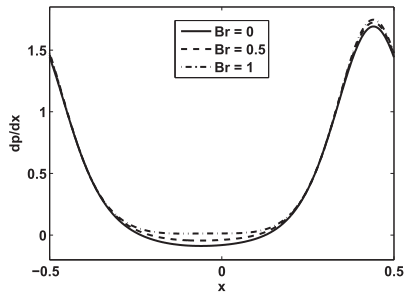

(b) N_b=0.8, N_t=1.5, M=1, α=0.2, Pr=3, G_t=0.9, G_c=0.4, λ_1=0.5

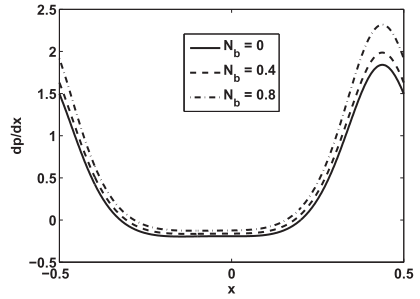

(c) N_t=0.9, Br=0.5, M=1, α=0.4, Pr=3, G_t=0.8, G_c=0.2, λ_1=0.1

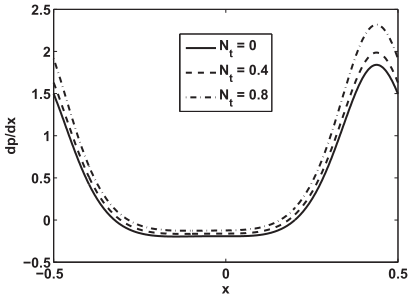

(d) N_b=0.8, Br=0.5, M=1, α=0.2, Pr=3, G_t=0.8, G_c=0.4, λ_1=0.1

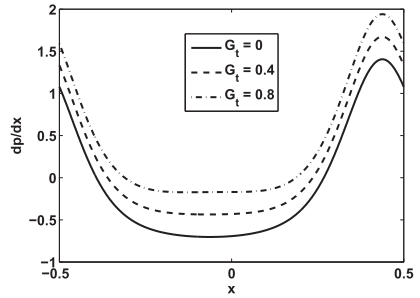

(e) N_b=0.8, N_t=0.3, M=1, Pr=3, Br=0.5, α=0.2, G_c=0.2, λ_1=0.1

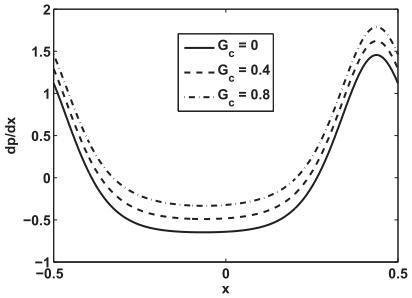

(f) N_t=0.3, N_b=0.8, Br=5, M=1, α=0.2, Pr=3, G_t=0.2, λ_1=0.1

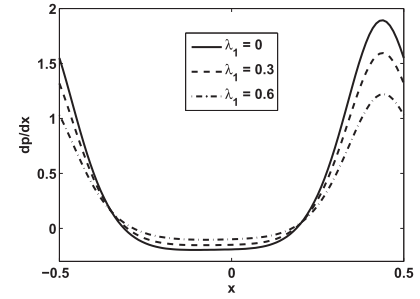

(g) N_b=0.3, N_t=0.4, Br=0.5, M=1, α=0.4, Pr=3, G_t=0.8, G_c=0.2

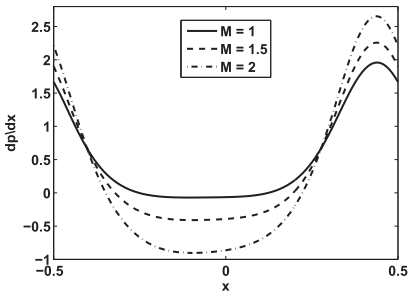

(h) N_b=0.7, N_t=0.8, α=0.4, Pr=3, Br=0.5, G_t=0.8, G_c=0.3, λ_1=0.1

Fig. 3. Pressure gradient dp/dx versus x for a_1=0.5, d = 1.5, $a_2 = 0.5$, $\phi = \pi/4$, Q = 0.5.

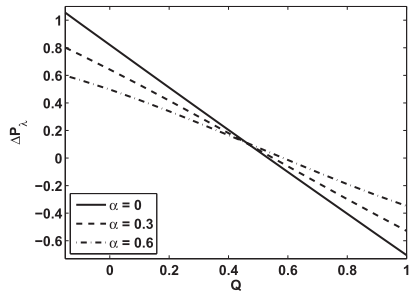

(a) N_b=0.3, N_t=0.8, M=1, Pr=3, Br=1.5, G_t=0.2, G_c=0.2, λ_1=0.1

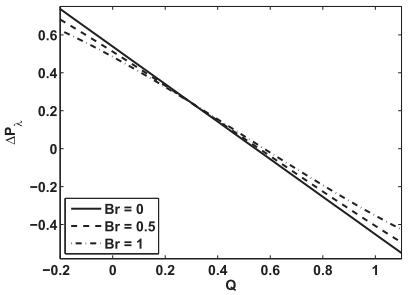

(b) N_b=0.3, N_t=0.8, M=1, α=0.7, Pr=3, G_t=0.2, G_c=0.2, λ_1=0.1

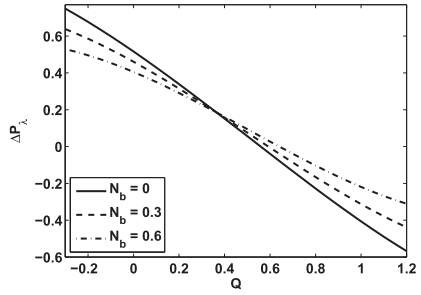

(c) Br=1, N_t=0.8, M=1, α=0.7, Pr=3, G_t=0.2, G_c=0.2, λ_1=0.1

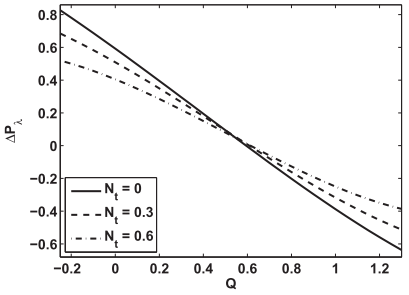

(d) N_b=0.7, Br=1, M=1, α=0.7, Pr=3, G_t=0.2, G_c=0.2, λ_1=0.1

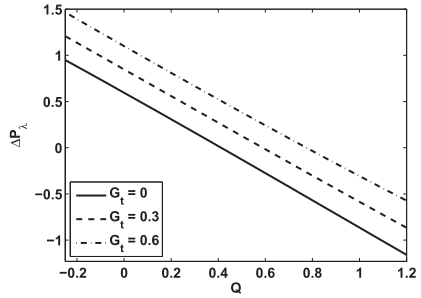

(e) N_b=0.2, N_t=0.8, Br=1, M=1, α=0.1, Pr=3, G_c=0.2, λ_1=0.1

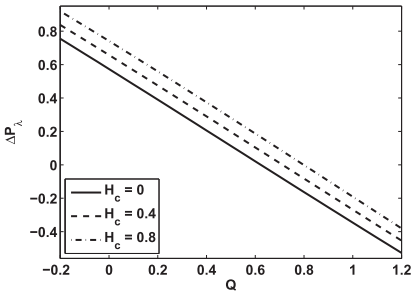

(f) N_b=0.2, N_t=0.8, M=1, Pr=3, Br=0.3, α=0.1, G_t=0.2, λ_1=0.1

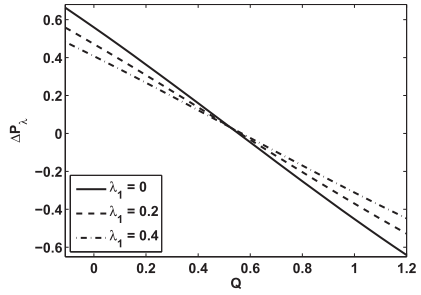

(g) N_b=0.3, N_t=0.8, Pr=3, M=1, Br=0.5, α=0.7, G_t=0.2, G_c=0.2

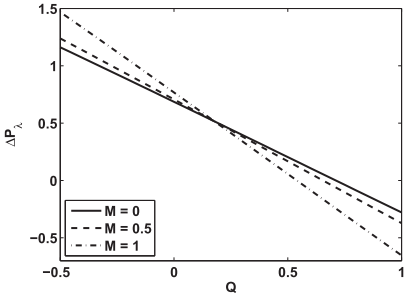

(h) N_b=0.7, N_t=0.8, Pr=3, α=0.1, Br=0.5, G_t=0.2, G_c=0.2, λ_1=0.1

Fig. 4. Pressure rise ΔP_λ versus flow rate Q for $a_1 = 0.5$, $d = 1.5$, $a_2 = 0.5$, $\phi = \pi/4$.

Table 3
Critical values of Q for which $\Delta P_\lambda = 0$.

α	Q_0	Br	Q_0	N_b	Q_0	N_t	Q_0
0.0	0.5336	0.0	0.5440	0.0	0.5589	0.0	0.5939
0.3	0.5503	0.5	0.5561	0.3	0.5922	0.3	0.6083
0.6	0.5843	1.0	0.5765	0.6	0.6405	0.6	0.6137
G_t	Q_0	G_c	Q_0	λ_1	Q_0	M	Q_0
0.0	0.4118	0.0	0.6226	0.0	0.5546	0.0	0.7110
0.3	0.5890	0.3	0.7116	0.2	0.5612	0.5	0.6549
0.6	0.7741	0.6	0.7985	0.4	0.5675	1.0	0.5395

Table 4
Values of ΔP_λ for which $Q = 0$.

α	P_0	Br	P_0	N_b	P_0	N_t	P_0
0.0	0.8217	0.0	0.5384	0.0	0.5162	0.0	0.5923
0.3	0.6422	0.5	0.5116	0.3	0.4605	0.3	0.5090
0.6	0.4975	1.0	0.4845	0.6	0.4052	0.6	0.4048
G_t	P_0	G_c	P_0	λ_1	P_0	M	P_0
0.0	0.5948	0.0	0.5734	0.0	0.5594	0.0	0.6863
0.3	0.8469	0.3	0.6573	0.2	0.4715	0.5	0.7069
0.6	1.0990	0.6	0.7412	0.4	0.4078	1.0	0.7680

Conclusion

Mixed convective peristaltic flow of Jeffrey nanofluid variable viscosity is studied with the consideration of viscous dissipation and Joule heating effects. The findings of the present paper can be summarized as: There exists a linear relationship between ΔP_λ and Q for G_t, G_c, λ_1 and M but nonlinear relationship occurs for α, Br, N_b and N_t. An increase in α, Br, N_b, N_t and λ_1 leads to a fall in peristaltic and retrograde pumping rates and a rise in copumping rate. The amplitude of velocity and temperature profiles increases with the consideration of nanoparticles in the fluid, but opposite is true for concentration profile. The fluid concentration is higher for variable viscosity fluid as compared to constant viscosity fluid. The trapped bolus in the right side of channel for increasing α, G_t and G_c shows a reversed behavior when compared with bolus in the left side of the channel.

Appendix A

In view of Eqs. (30)–(32), one can obtain family of equations corresponding to Eqs. (21)–(23) as given below

$$(1-j)\mathcal{L}_\psi[\hat{\psi}(y;j)-\psi_0(y)] = j\hbar_\psi \mathcal{N}_\psi[\hat{\psi}(y;j),\hat{\theta}(y;j)], \tag{A-1}$$

$$(1-j)\mathcal{L}_\theta[\hat{\theta}(y;j)-\theta_0(y)] = j\hbar_\theta \mathcal{N}_\theta[\hat{\psi}(y;j),\hat{\theta}(y;j),\hat{\eta}(y;j)], \tag{A-2}$$

$$(1-j)\mathcal{L}_\eta[\hat{\eta}(y;j)-\eta_0(y)] = j\hbar_\eta \mathcal{N}_\eta[\hat{\theta}(y;j),\hat{\eta}(y;j)], \tag{A-3}$$

called the zeroth-order deformation equations, whose solution varies continuously with respect to embedded parameter $j \in [0,1]$. Here $\hbar_\psi, \hbar_\theta$ and $\hbar_\eta$ are the non-zero auxiliary parameters.

$$\hat{\psi}(y;j) = F/2, \frac{\partial\hat{\psi}(y;j)}{\partial y} = -1, \hat{\theta}(y;j) = 0, \hat{\eta}(y;j) = 0, \quad at \quad y = h_1, \tag{A-4}$$

$$\hat{\psi}(y;j) = -F/2, \frac{\partial\hat{\psi}(y;j)}{\partial y} = -1, \hat{\theta}(y;j) = 1, \hat{\eta}(y;j) = 1, \quad at \quad y = h_2. \tag{A-5}$$

The non-linear operators are given by

$$\begin{aligned}\mathcal{N}_\psi[\hat{\psi}(y;j),\hat{\theta}(y;j),\hat{\eta}(y;j)] &= \frac{\partial^4\hat{\psi}(y;j)}{\partial y^4} - (1+\lambda_1)M^2\frac{\partial^2\hat{\psi}(y;j)}{\partial y^2} \\ &- \alpha\left[\hat{\theta}(y;j)\frac{\partial^4\hat{\psi}(y;j)}{\partial y^4} + 2\frac{\partial\hat{\theta}(y;j)}{\partial y}\frac{\partial^3\hat{\psi}(y;j)}{\partial y^3} + \frac{\partial^2\hat{\theta}(y;j)}{\partial y^2}\frac{\partial^2\hat{\psi}(y;j)}{\partial y^2}\right] \\ &+ (1+\lambda_1)\left[G_t\frac{\partial\hat{\theta}(y;j)}{\partial y} + G_c\frac{\partial\hat{\eta}(y;j)}{\partial y}\right],\end{aligned} \tag{A-6}$$

$$\begin{aligned}\mathcal{N}_\theta[\hat{\psi}(y;j),\hat{\theta}(y;j),\hat{\eta}(y;j)] &= \frac{\partial^2\hat{\theta}(y;j)}{\partial y^2} \\ &+ \frac{\mathrm{Br}}{(1+\lambda_1)}\left[\left(\frac{\partial^2\hat{\psi}(y;j)}{\partial y^2}\right)^2 - \alpha\hat{\theta}(y;j)\left(\frac{\partial^2\hat{\psi}(y;j)}{\partial y^2}\right)^2\right] \\ &+ \mathrm{Br}M^2\left[\left(\frac{\partial\hat{\psi}(y;j)}{\partial y}\right)^2 + 2\frac{\partial\hat{\psi}(y;j)}{\partial y}\right] + \mathrm{Pr}N_b\frac{\partial\hat{\theta}(y;j)}{\partial y}\frac{\partial\hat{\eta}(y;j)}{\partial y} \\ &+ \mathrm{Pr}N_t\left(\frac{\partial\hat{\theta}(y;j)}{\partial y}\right)^2 + \mathrm{Br}M^2(1-\chi_m),\end{aligned} \tag{A-7}$$

$$\mathcal{N}_\eta[\hat{\psi}(y;j),\hat{\theta}(y;j),\hat{\eta}(y;j)] = \frac{\partial^2\hat{\eta}(y;j)}{\partial y^2} + \frac{N_t}{N_b}\frac{\partial^2\hat{\theta}(y;j)}{\partial y^2}. \tag{A-8}$$

For $j = 0$ and $j = 1$, we get

$$\begin{aligned}\hat{\psi}(y;0) = \psi_0(y), \quad \hat{\theta}(y;0) = \theta_0(y), \quad \hat{\eta}(y;0) = \eta_0(y), \\ \hat{\psi}(y;1) = \psi(y), \quad \hat{\theta}(y;1) = \theta(y), \quad \hat{\eta}(y;1) = \eta(y).\end{aligned} \tag{A-9}$$

As the embedded parameter j increases from zero to unity, $\hat{\psi}(y,j), \hat{\theta}(y,j)$ and $\hat{\eta}(y,j)$ differ from $\psi_0(y), \theta_0(y)$ and $\eta_0(y)$ i.e initial guesses to $\psi(y), \theta(y)$ and $\eta(y)$ i.e solution. Using Taylor's expansion one can write

$$\hat{\psi}(y,j) = \psi_0(y) + \sum_{m=1}^{\infty}\hat{\psi}_m(y)j^m, \quad \hat{\psi}_m(y) = \frac{1}{m!}\frac{\partial^m\hat{\psi}(y;j)}{\partial j^m}, \tag{A-10}$$

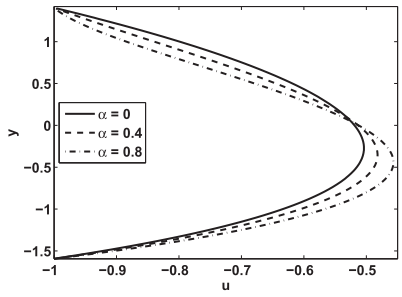

(a) N_b=1.2, N_t=0.7, M=1, Br=2, Pr=6, G_t=0.2, G_c=0.5, λ_1=0.1

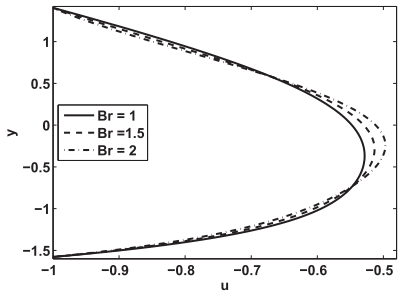

(b) N_b=0.5, N_t=0.8, M=2, α=0.9, Pr=6, G_t=0.2, G_c=0.5, λ_1=0.1

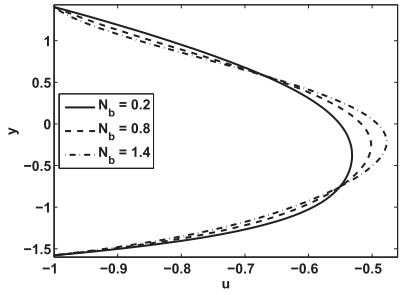

(c) N_t=1.2, M=2, Br=1.5, α=0.9, Pr=3, G_t=0.2, G_c=0.5, λ_1=0.1

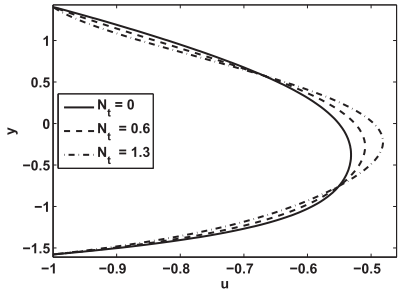

(d) N_b=1.2, M=2, Br=1.5, Pr=3, α=0.6, G_t=0.2, G_c=0.5, λ_1=0.1

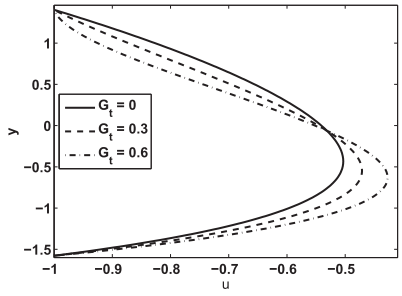

(e) N_b=1, N_t=0.7, M=1, Br=0.3, α=0.6, Pr=3, G_c=0.5, λ_1=0.1

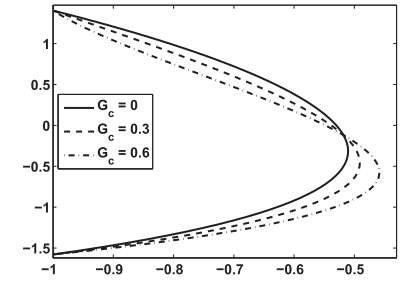

(f) N_b=0.5, N_t=0.8, M=2, Pr=3, Br=0.3, α=0.3, G_t=0.5, λ_1=0.1

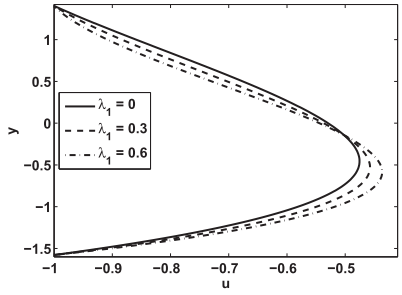

(g) N_b=0.9, N_t=0.8, M=2, Br=1, Pr=3, α=0.5, G_t=0.2, G_c=0.5

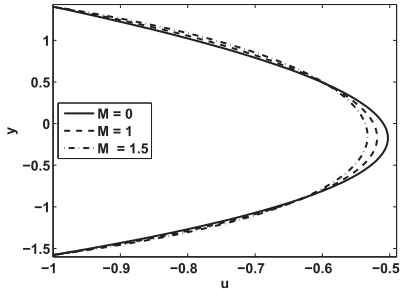

(h) N_b=0.3, N_t=0.7, Br=2, α=0.2, Pr=3, G_t=0.1, G_c=0.1, λ_1=0.1

Fig. 5. Velocity u versus y for $a_1 = 0.5$, $d = 1.5$, $a_2 = 0.5$, $x = 0.1$, $\phi = \pi/4$, $Q = 0.5$.

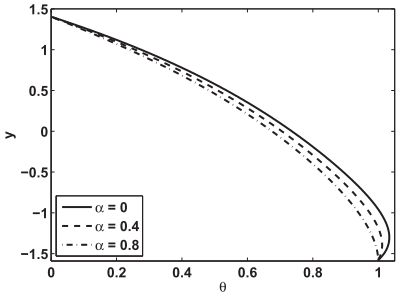

(a) N_t=0.7, N_b=0.8, Br=1, Pr=3, M=0.5, G_t=0.5, G_c=0.5, λ_1=0.1

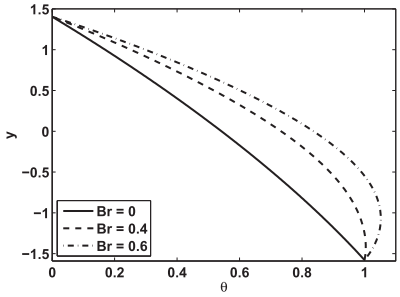

(b) N_t=0.7, N_b=0.8, Pr=3, M=1, α=0.3, G_t=0.5, G_c=0.2, λ_1=0.3

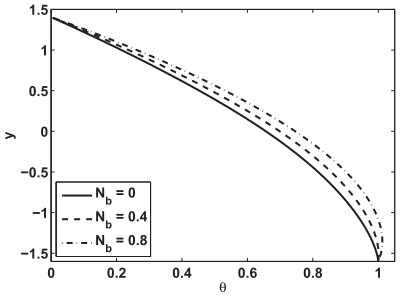

(c) N_t=0.7, M=1, Br=0.5, Pr=3, α=0.3, G_t=0.5, G_c=0.2, λ_1=0.1

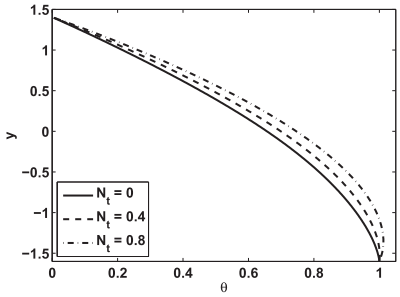

(d) N_b=0.7, M=1, Br=0.8, α=0.3, Pr=3, G_t=0.5, G_c=0.2, λ_1=0.3

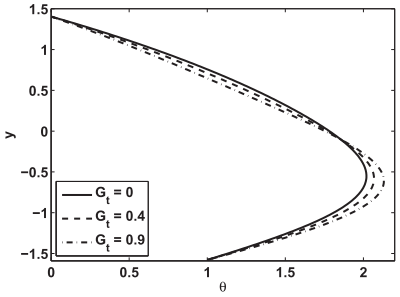

(e) N_t=0.2, N_b=0.7, M=2, Pr=3, α=0.5, Br=2, G_c=0.7, λ_1=0.4

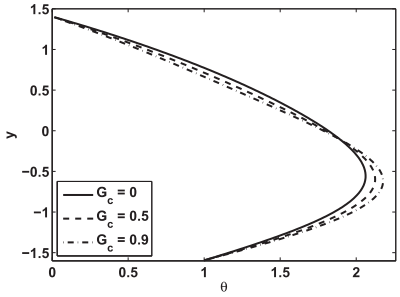

(f) N_t=0.2, N_b=0.7, M=2, Br=2, α=0.5, Pr=3, G_t=0.7, λ_1=0.4

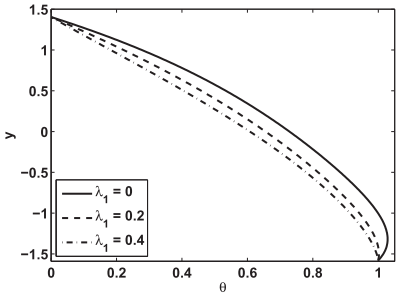

(g) N_b=0.8, N_t=0.2, Pr=3, Br=2, M=0.5, α=0.2, G_t=0.5, G_c=0.2

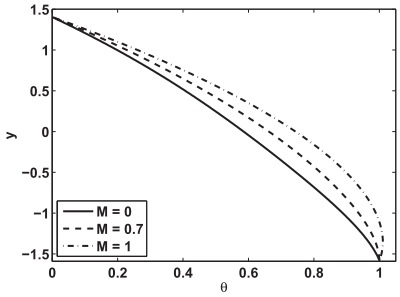

(h) N_t=0.7, N_b=0.8, Pr=3, α=0.3, Br=0.8, G_t=0.5, G_c=0.2, λ_1=0.3

Fig. 6. Temperature profile θ versus y for $a_1 = 0.5$, $d = 1.5$, $a_2 = 0.5$, $x = 0.1$, $Q = 0.5$, $\phi = \pi/4$.

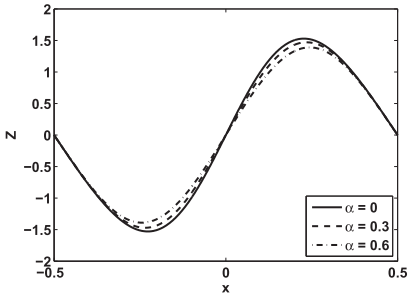

(a) N_t=0.9, N_b=0.3, Pr=3, Br=1, M=0.5, G_t=0.5, G_c=0.4, λ_1=0.5

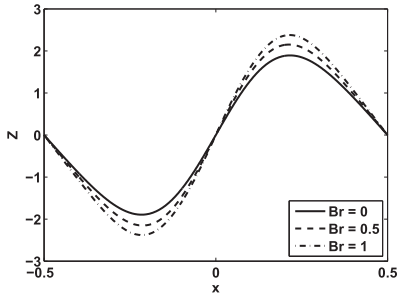

(b) N_t=0.9, M=0.5, Pr=3, α=0.1, N_b=0.7, G_t=0.5, G_c=0.4, λ_1=0.1

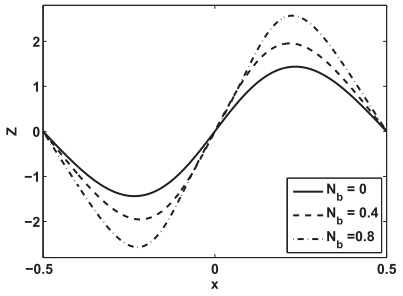

(c) N_t=0.9, M=1, Br=0.5, α=0.1, Pr=3, G_t=0.5, G_c=0.4, λ_1=0.1

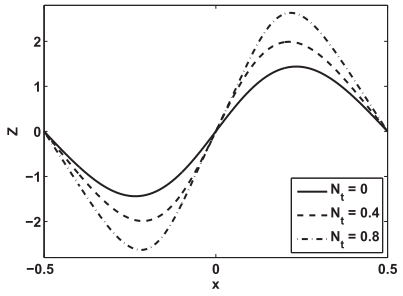

(d) N_b=0.9, M=1, Br=0.5, α=0.1, Pr=3, G_t=0.5, G_c=0.4, λ_1=0.1

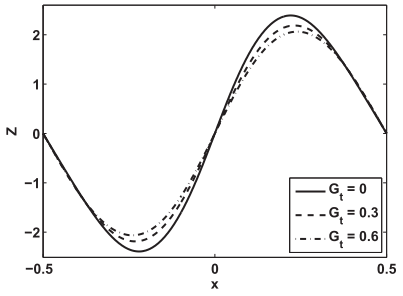

(e) N_t=0.5, N_b=0.9, Pr=3, M=2, α=0.5, Br=0.5, G_c=0.4, λ_1=0.5

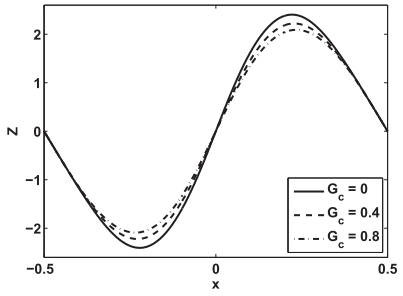

(f) N_t=0.5, N_b=0.9, M=2, Pr=3, Br=0.5, α=0.5, G_t=0.4, λ_1=0.5

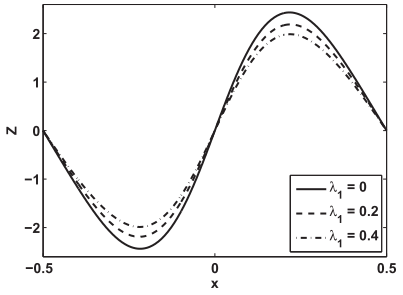

(g) N_b=0.9, N_t=0.5, M=2, Pr=3, Br=0.5, α=0.5, G_t=0.5, G_c=0.4

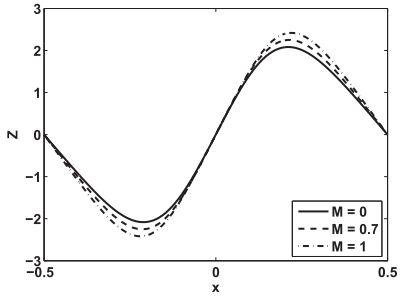

(h) N_t=0.9, N_b=0.7, Pr=3, α=0.1, Br=0.5, G_t=0.5, G_c=0.4, λ_1=0.1

Fig. 7. Heat transfer coefficient Z versus x for $a_1 = 0.5$, $d = 1.5$, $a_2 = 0.5$, $Q = 0.5$, $\phi = \pi/4$.

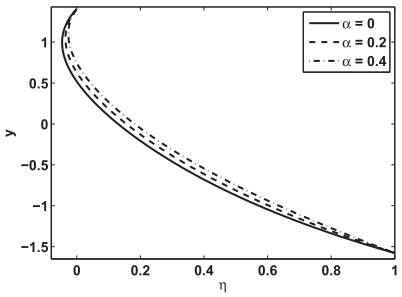

(a) N_b=0.7, N_t=0.8, M=0.5, Br=2, Pr=3, G_t=0.5, G_c=0.4, λ_1=0.1

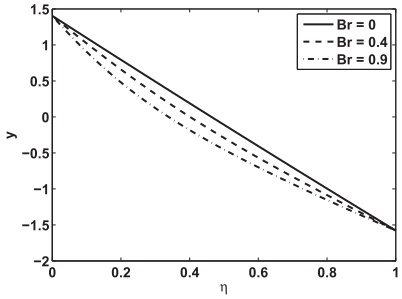

(b) N_b=0.8, N_t=0.3, M=2, α=0.3, Pr=3, G_t=0.1, G_c=0.1, λ_1=0.1

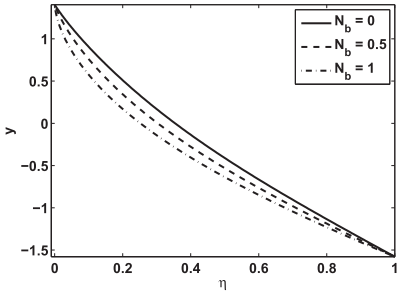

(c) N_t=1, M=1, Br=0.6, α=0.5, Pr=3, G_t=0.1, G_c=0.1, λ_1=0.1

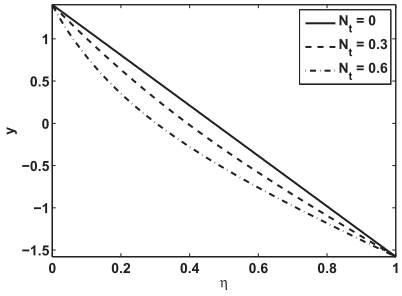

(d) N_b=0.7, M=1.5, Br=1, Pr=3, α=0.5, G_t=0.1, G_c=0.1, λ_1=0.1

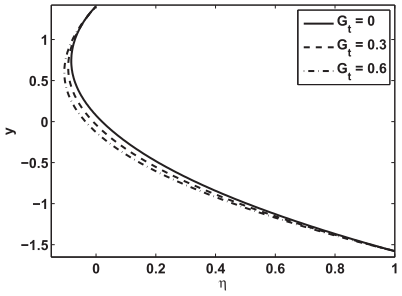

(e) N_b=1, N_t=0.5, M=1.8, Br=1, α=0.1, Pr=3, G_c=0.4, λ_1=0.3

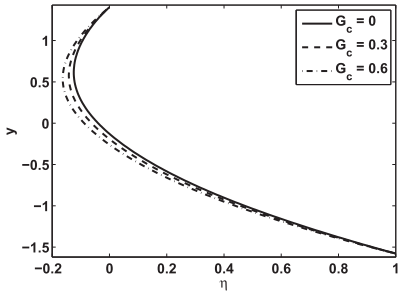

(f) N_t=0.5, N_b=0.9, M=2, Pr=3, Br=0.9, α=0.1, G_t=0.4, λ_1=0.8

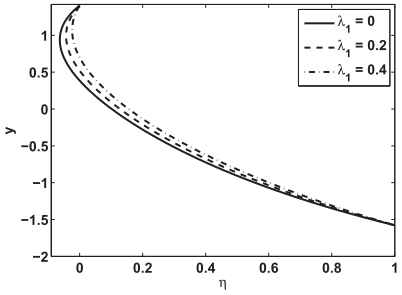

(g) N_b=0.8, N_t=0.7, M=0.5, Br=2, Pr=3, α=0.1, G_t=0.8, G_c=0.5

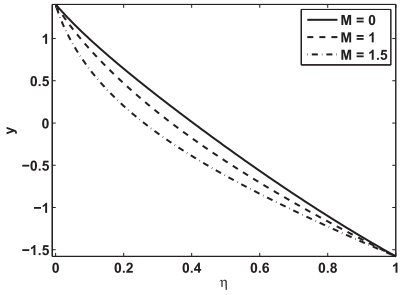

(h) N_b=0.7, N_t=0.7, Br=0.5, α=0.3, Pr=3, G_t=0.1, G_c=0.1, λ_1=0.1

Fig. 8. Concentration η versus y for $a_1 = 0.5$, $d = 1.5$, $a_2 = 0.5$, $x = 0.1$, $\phi = \pi/4$, $Q = 0.5$.

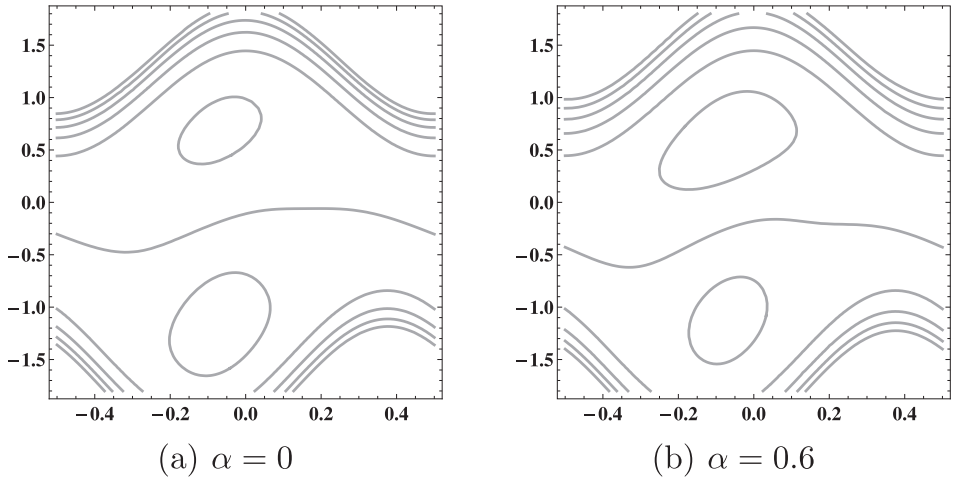

Fig. 9. Streamlines for variation of α for $a_1 = 0.5$, $d = 1.5$, $a_2 = 0.5$, $Q = 2.4$, $\phi = \pi/4$, $N_b = 0.7$, $N_t = 0.8$, $M = 3$, Pr = 3, Br = 0.3, $G_t = 0.3$, $G_c = 0.4$, $\lambda_1 = 0.1$.

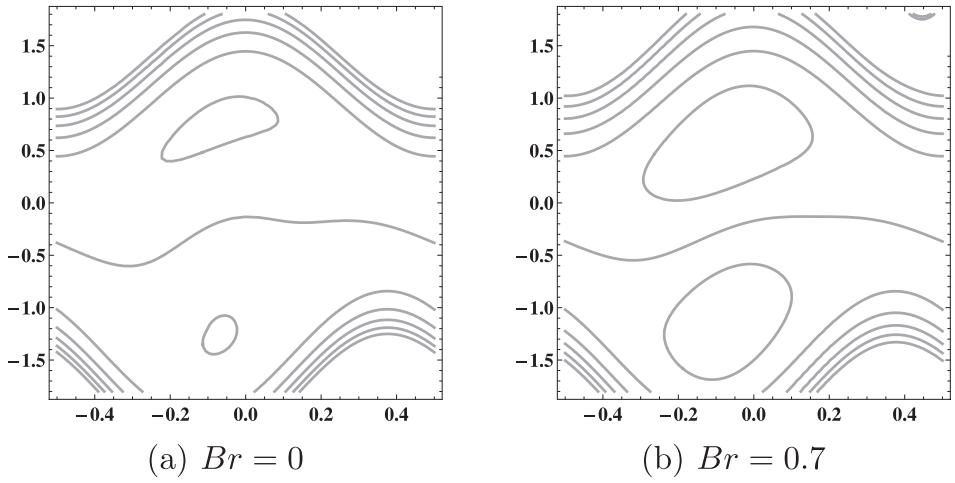

Fig. 10. Streamlines for variation of Br for $a_1 = 0.5$, $d = 1.5$, $a_2 = 0.5$, $Q = 2.4$, $\phi = \pi/4$, $N_b = 0.7$, $N_t = 0.8$, $M = 2$, $\alpha = 0.3$, Pr = 3, $G_t = 0.3$, $G_c = 0.4$, $\lambda_1 = 0.5$.

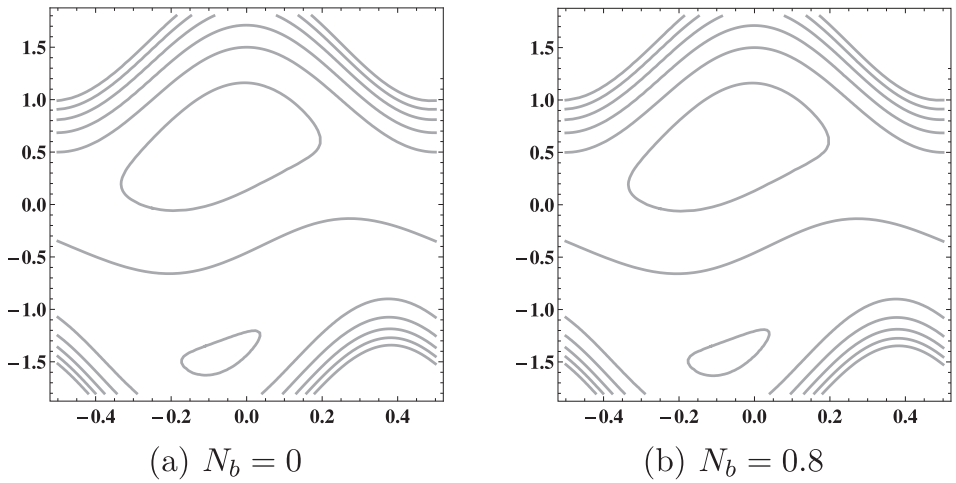

Fig. 11. Streamlines for variation of N_b for $a_1 = 0.5$, $d = 1.5$, $a_2 = 0.5$, $Q = 2.4$, $\phi = \pi/4$, $N_t = 0.7$, $M = 1$, Br = 0.3, $\alpha = 0.1$, Pr = 3, $G_t = 0.3$, $G_c = 0.4$, $\lambda_1 = 0.4$.

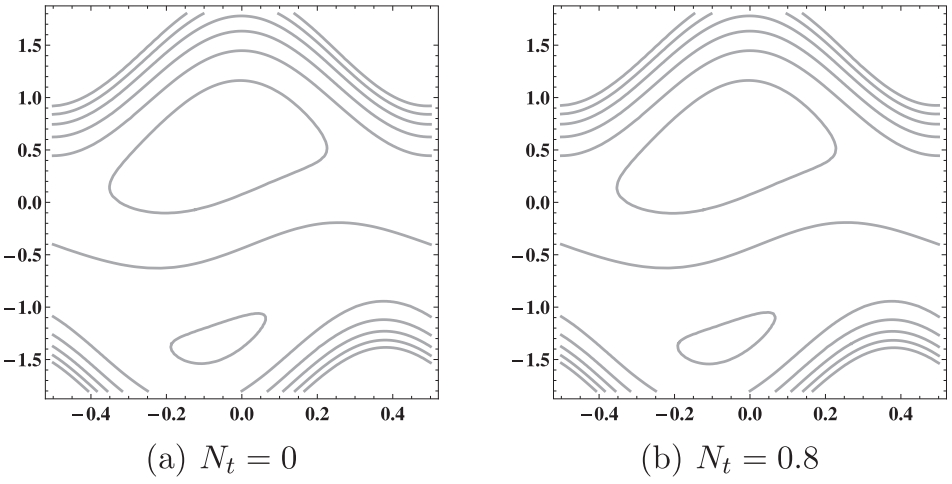

Fig. 12. Streamlines for variation of N_t for a_1=0.5, a_2=0.5, d = 1.5, Q = 2.4, ϕ=π/4, N_b=0.7, M = 1, Br = 0.3, Pr = 3, α=0.2, G_t=0.3, G_c=0.4, λ_1=0.4

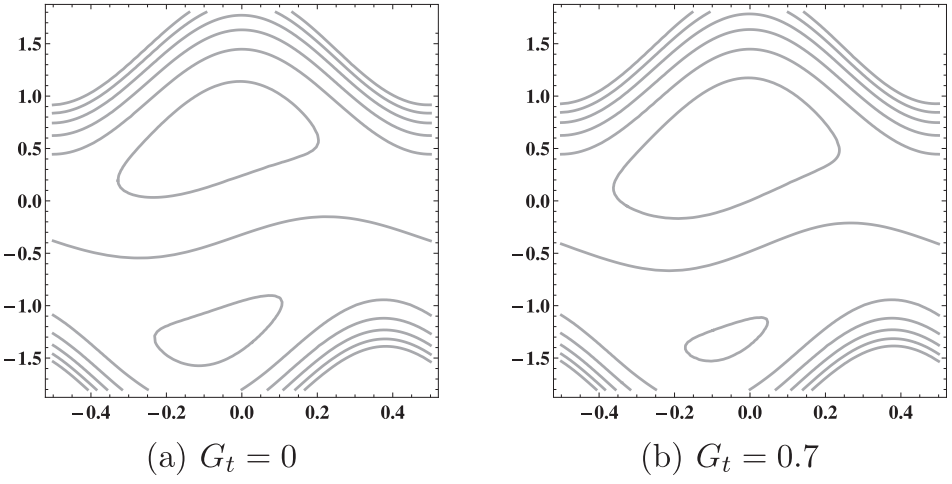

Fig. 13. Streamlines for variation of G_t for $a_1 = 0.5$, d = 1.5, $a_2 = 0.5$, Q = 2.4, $\phi = \pi/4$, $N_t = 0.3$, $N_b = 0.8$, Pr = 3, M = 1, $\alpha = 0.2$, Br = 0.3, $G_c = 0.2$, $\lambda_1 = 0.5$.

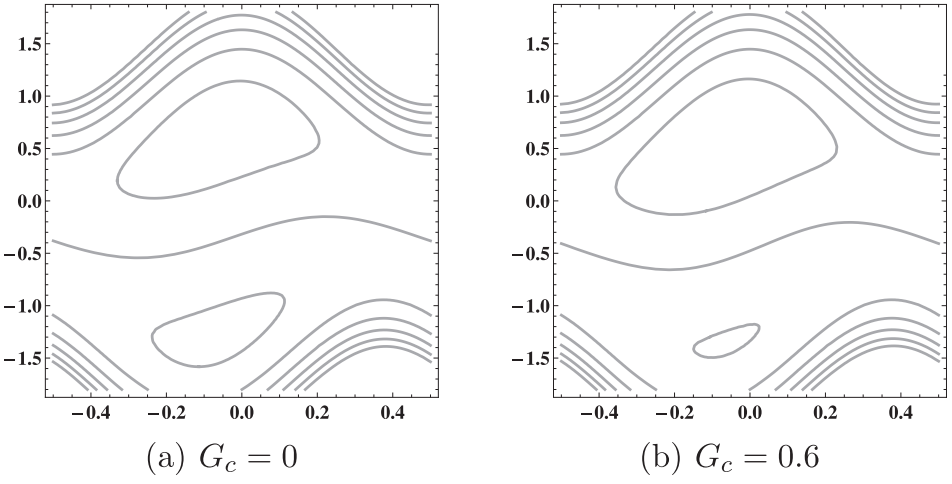

Fig. 14. Streamlines for variation of G_c for $a_1 = 0.5$, d = 1.5, $a_2 = 0.5$, Q = 2.4, $\phi = \pi/4$, $N_t = 0.3$, $N_b = 0.8$, M = 1, Pr = 3, Br = 0.3, $\alpha = 0.2$, $G_t = 0.2$, $\lambda_1 = 0.5$.

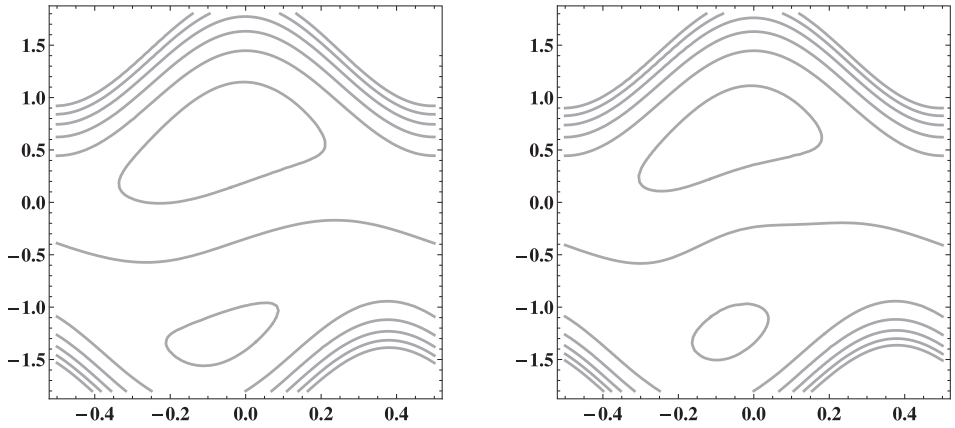

Fig. 15. Streamlines for variation of λ_1 for $a_1 = 0.5$, $d = 1.5$, $a_2 = 0.5$, $Q = 2.4$, $\phi = \pi/4$, $N_b = 0.7$, $N_t = 0.8$, $M = 1.5$, Br = 0.3, Pr = 3, $\alpha = 0.2$, $G_t = 0.3$, $G_c = 0.4$.

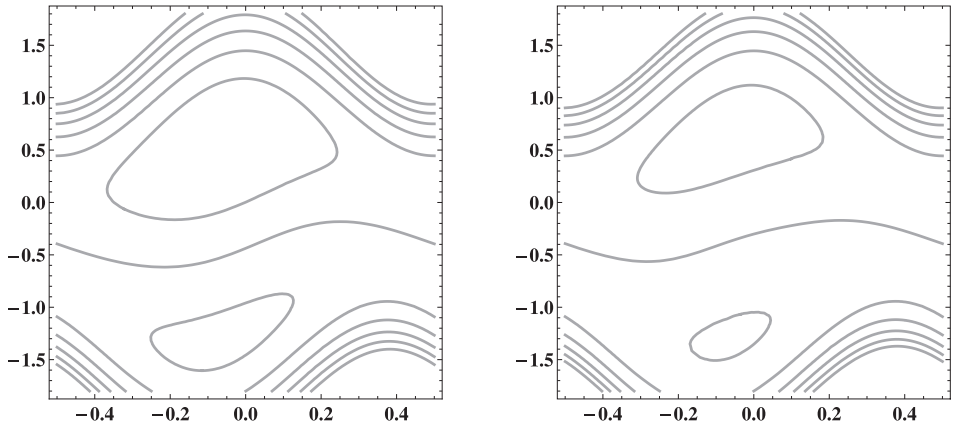

Fig. 16. Streamlines for variation of M for $a_1 = 0.5$, $d = 1.5$, $a_2 = 0.5$, $Q = 2.4$, $\phi = \pi/4$, $N_b = 0.7$, $N_t = 1$, Br = 0.5, $\alpha = 0.3$, Pr = 3, $G_t = 0.1$, $G_c = 0.1$, $\lambda_1 = 0.1$.

$$\hat{\theta}(y,j) = \theta_0(y) + \sum_{m=1}^{\infty} \hat{\theta}_m(y) j^m, \quad \hat{\theta}_m(y) = \frac{1}{m!} \frac{\partial^m \hat{\theta}(y;j)}{\partial j^m}, \tag{A-11}$$

$$\hat{\eta}(y,j) = \eta_0(y) + \sum_{m=1}^{\infty} \hat{\eta}_m(y) j^m, \quad \hat{\eta}_m(y) = \frac{1}{m!} \frac{\partial^m \hat{\eta}(y;j)}{\partial j^m}. \tag{A-12}$$

If the auxiliary linear operators, initial guesses and auxiliary parameters are chosen properly, the above series converges for $j = 1$. Hence

$$\hat{\psi}(y) = \psi_0(y) + \sum_{m=1}^{\infty} \hat{\psi}_m(y), \tag{A-13}$$

$$\hat{\theta}(y) = \theta_0(y) + \sum_{m=1}^{\infty} \hat{\theta}_m(y), \tag{A-14}$$

$$\hat{\eta}(y) = \eta_0(y) + \sum_{m=1}^{\infty} \hat{\eta}_m(y). \tag{A-15}$$

Deformation equations of mth order are obtained by differentiating Eqs. (A-1) to (A-3) m times wrt j, divide by $m!$ and set $j = 0$

$$\mathcal{L}_{\psi}[\hat{\psi}_m - \chi_m \hat{\psi}_{m-1}(y)] = \hbar_{\psi} \mathcal{R}^{\psi}_m(y), \tag{A-16}$$

$$\mathcal{L}_{\theta}[\hat{\theta}_m - \chi_m \hat{\theta}_{m-1}(y)] = \hbar_{\theta} \mathcal{R}^{\theta}_m(y), \tag{A-17}$$

$$\mathcal{L}_{\eta}[\hat{\eta}_m - \chi_m \hat{\eta}_{m-1}(y)] = \hbar_{\eta} \mathcal{R}^{\eta}_m(y), \tag{A-18}$$

with boundary conditions

$$\hat{\psi}_m(y;j) = F/2, \ \frac{\partial \hat{\psi}_m(y;j)}{\partial y} = -1, \ \ \hat{\theta}_m(y;j) = 0, \\ \hat{\eta}_m(y;j) = 0, \qquad at \quad y = h_1, \tag{A-19}$$

$$\hat{\psi}_m(y;j) = -F/2, \ \frac{\partial \hat{\psi}_m(y;j)}{\partial y} = -1, \ \ \hat{\theta}_m(y;j) = 1, \\ \hat{\eta}_m(y;j) = 1, \qquad at \quad y = h_2, \tag{A-20}$$

where

$$\mathcal{R}^{\psi}_m(y) = \frac{\partial^4 \hat{\psi}_{m-1}}{\partial y^4} - \alpha \sum_{k=0}^{m-1} \left[\hat{\theta}_{m-1-k}(y) \frac{\partial^4 \hat{\psi}_k}{\partial y^4} + 2 \frac{\partial \hat{\theta}_{m-1-k}}{\partial y} \frac{\partial^3 \hat{\psi}_k}{\partial y^3} + \frac{\partial^2 \hat{\theta}_{m-1-k}}{\partial y^2} \frac{\partial^2 \hat{\psi}_k}{\partial y^2} \right] \\ - (1+\lambda_1) M^2 \frac{\partial^2 \hat{\psi}_{m-1}}{\partial y^2} + (1+\lambda_1) \left[G_t \frac{\partial \hat{\theta}_{m-1}}{\partial y} + G_c \frac{\partial \hat{\eta}_{m-1}}{\partial y} \right], \tag{A-21}$$

$$\mathcal{R}_m^{\theta}(y) = \frac{\partial^2 \hat{\theta}_{m-1}}{\partial y^2} + \mathrm{Br}M^2 \left[\sum_{k=0}^{m-1} \frac{\partial \hat{\psi}_{m-1-k}}{\partial y} \frac{\partial \hat{\psi}_k}{\partial y} + 2 \frac{\partial \hat{\psi}_{m-1}(y)}{\partial y} \right] + \mathrm{Br}M^2 (1 - \chi_m) + \frac{\mathrm{Br}}{(1+\lambda_1)} \sum_{k=0}^{m-1} \left[\frac{\partial^2 \hat{\psi}_{m-1-k}}{\partial y^2} \frac{\partial^2 \hat{\psi}_k}{\partial y^2} - \alpha \sum_{l=0}^{k} \hat{\theta}_{m-1-k} \frac{\partial^2 \hat{\psi}_{k-1}}{\partial y^2} \frac{\partial^2 \hat{\psi}_l}{\partial y^2} \right] + \mathrm{Pr}N_b \sum_{k=0}^{m-1} \frac{\partial \hat{\theta}_{m-1-k}}{\partial y} \frac{\partial \hat{\eta}_k}{\partial y} + \mathrm{Pr}N_t \sum_{k=0}^{m-1} \frac{\partial \hat{\theta}_{m-1-k}}{\partial y} \frac{\partial \hat{\theta}_k}{\partial y}, \tag{A-22}$$

$$\mathcal{R}_m^{\eta}(y) = \frac{\partial^2 \hat{\eta}_{m-1}}{\partial y^2} + \frac{N_t}{N_b} \frac{\partial^2 \hat{\theta}_{m-1}}{\partial y^2}, \tag{A-23}$$

and

$$\chi_m = \begin{cases} 0, & m \leqslant 1 \\ 1, & m > 1. \end{cases} \tag{A-24}$$

Solving the above mth order deformation problems, one obtains

$$\psi_m(y) = \psi_m^*(y) + C_1 + C_2 y + C_3 y^2 + C_4 y^3, \tag{A-25}$$

$$\theta_m(y) = \theta_m^*(y) + C_5 + C_6 y, \tag{A-26}$$

$$\eta_m(y) = \eta_m^*(y) + C_7 + C_8 y, \tag{A-27}$$

where $\psi_m^*(y), \theta_m^*(y)$ and $\eta_m^*(y)$ are special solutions.

References

[1] Shapiro A. Pumping and retrograde diffusion in peristaltic waves. Proceedings of a Workshop in Ureteral Reflux in Children. Washington D.C., USA: National Academy of Sciences; 1967. p. 109–26.

[2] Asghar S, Hussain Q, Hayat T, Alsaadi F. Hall and ion slip effects on peristaltic flow and heat transfer analysis with ohmic heating. Appl Math Mech (Engl Ed) 2014;35(12):1509–24.

[3] Srinivas S, Gayathri R. Peristaltic transport of a Newtonian fluid in a vertical asymmetric channel with heat transfer and porous medium. Appl Math Comput 2009;215:185–96.

[4] Tripathi D. A mathematical model for swallowing of food bolus through the oesophagus under the influence of heat transfer. Int J Therm Sci 2012;51:91–101.

[5] Hussain Q, Hayat T, Asghar S, Alsaadi F. Heat and mass transfer analysis in variable viscosity peristaltic flow with hall current and ion-slip. J Mech Med Biol 2016;16(4). Article ID: 1650047.

[6] Mekheimer K, Salem A, Zaher A. Peristatically induced MHD slip flow in a porous medium due to a surface acoustic wavy wall. J Egypt Math Soc 2014;22 (1):143–51.

[7] Hayat T, Ahmad N, Ali N. Effects of endoscope and magnetic field on the peristalsis involving Jeffrey fluid. Commun Nonlinear Sci Numer Simul 2008;13:1581–91.

[8] Hayat T, Rafiq M, Ahmad B. Influences of rotation and thermophoresis on MHD peristaltic transport of Jeffrey fluid with convective conditions and wall properties. J Magn Magn Mater 2016;410:89–99.

[9] Hayat T, Shafique M, Tanveer A, Alsaedi A. Hall and ion slip effects on peristaltic flow of Jeffrey nanofluid with Joule heating. J Magn Magn Mater 2016;407:51–9.

[10] Choi S. Enhancing thermal conductivity of fluids with nanoparticles. ASME Publ Fed 1995;231:99–106.

[11] Buongiorno J. Convective transport in nanofluids. ASME J Heat Transf 2005;128:240–50.

[12] Rashidi M, Bég O, Asadi M, Rastegari M. DTM-Padé modeling of natural convective boundary layer flow of a nanofluid past a vertical surface. Int J Therm Environ Eng 2012;4(1):13–24.

[13] Mustafa M, Farooq M, Hayat T, Alsaedi A. Numerical and series solutions for stagnation point flow of nanofluid over an exponentially stretching sheet. PLoS ONE 2013;8(5). Article ID: e61859.

[14] Hayat T, Asad S, Alsaedi A. Flow of Casson fluid with nanoparticles. Appl Math Mech (Engl Ed) 2016;37(4):459–70.

[15] Tripathi D, Bég O. A study on peristaltic flow of nanofluids: application in drug delivery systems. Int J Heat Mass Transf 2014;70:61–70.

[16] Kothandapani M, Prakash J. Effect of thermal radiation parameter and magnetic field on the peristaltic motion of Williamson nanofluids in a tapered asymmetric channel. Int J Heat Mass Transf 2015;81:234–45.

[17] Hayat T, Rashid M, Imtiaz M, Alsaedi A. Magnetohydrodynamic (MHD) flow of Cu-water nanofluid due to a rotating disk with partial slip. AIP Adv 2015;5(6). Article-ID: 067169.

[18] Ellahi R, Zeeshan A, Vafai K, Rahman HU. Series solutions for magnetohydrodynamic flow of non-newtonian nanofluid and heat transfer in coaxial porous cylinder with slip conditions. Proc Inst Mech Eng, Part N: J Nanoeng Nanosyst 2011;225(5):123–32.

[19] Mekheimer K, Elmaboud YA. Simultaneous effects of variable viscosity and thermal conductivity on peristaltic flow in a vertical asymmetric channel. Can J Phys 2014;92(12):1541–55.

[20] Hussain Q, Asghar S, Hayat T, Alsaedi A. Peristaltic transport of hydromagnetic Jeffrey fluid with temperature dependent viscosity and thermal conductivity. Int J Boimath 2016;9(2). Article ID: 1650029.

[21] Tanner R. Engineering rheology. Oxford Science Publications; 1985.

[22] Srivastava L, Srivastava V. Peristaltic transport of a power law fluid: Applications to the ductus efferentes of the reproductive tract. Rheol Acta 1988;27:428–33.

[23] Liao S. The proposed homotopy analysis technique for the solution of nonlinear problems. Shanghai Jiao Tong University; 1992 [Ph.D. dissertation].